Continuum Mech. Thermodyn. (2026) 38:86
https://doi.org/10.1007/s00161-026-01520-1

ORIGINAL ARTICLE

Yiheng Huang · Loredana Kehrer · Valerian Hirschberg · Eike Reinhardt · Frank Burbulla · Thomas Böhlke

Thermal history-dependent thermomechanical response of talc-filled and unfilled polypropylene

Received: 5 March 2026 / Accepted: 4 August 2026

Abstract The thermomechanical response of semicrystalline polypropylene (PP) depends not only on temperature and loading conditions, but also on its prior thermal state. While structural changes, such as post-crystallization and physical aging, induced by annealing treatments are well documented, their combined influence on thermal expansion, thermomechanical viscoelastic response, and crystalline fraction under service-relevant conditions in an automotive context remains inadequately quantified. In this study, unconditioned and thermally preconditioned unfilled and talc-filled PP were investigated by dilatometry, dynamic mechanical analysis, and differential scanning calorimetry over temperature and frequency ranges that are representative of service-relevant conditions. Thermal preconditioning resulted in a modification of the temperature-dependent coefficient of thermal expansion, as well as alterations in stiffness and damping levels. However, the glass transition temperature and the high-temperature α^*-relaxation remained predominantly unaltered. These alterations occurred in conjunction with an increase in the crystalline fraction, indicating a modified structural condition subsequent to thermal treatment. The talc-filled grades exhibited a lower overall level of thermal expansion, higher stiffness and crystallinity, and an effect on the high-temperature relaxation associated with the crystalline phase, without influencing the glass transition temperature. The findings demonstrate that thermal history modifies the structural state of polypropylene (PP) and is accompanied by changes in thermal expansion and dynamic viscoelastic response in both filled and unfilled systems. This is essential for constrained automotive exterior assemblies, which require dimensional stability and tolerance retention.

Keywords Talc-filled polypropylene · Coefficient of thermal expansion · Dynamic mechanical analysis · Differential scanning calorimetry · Thermal aging

Y. Huang · L. Kehrer · T. Böhlke (✉)
Institute of Engineering Mechanics, Continuum Mechanics (ITM-KM), Karlsruhe Institute of Technology (KIT), Kaiserstraße 10, 76131 Karlsruhe, Baden-Württemberg, Germany
E-mail: thomas.boehlke@kit.edu

Y. Huang
E-mail: yiheng.huang@partner.kit.edu; yiheng.huang2@porsche.de

L. Kehrer
E-mail: loredana.kehrer@kit.edu

Y. Huang · E. Reinhardt · F. Burbulla
Dr. Ing. h.c. F. Porsche AG, Porschestraße 911, 71287 Weissach, Baden-Württemberg, Germany
E-mail: eike.reinhardt@porsche.de

F. Burbulla
E-mail: frank.burbulla@porsche.de

V. Hirschberg
Institute of Technical Chemistry, Clausthal University of Technology, Agricolastrasße 4, 38678 Clausthal-Zellerfeld, Lower Saxony, Germany
E-mail: valerian.hirschberg@tu-clausthal.de

Published online: 19 August 2026

1 Introduction

Talc-filled polypropylene Plastics have become an integral component of modern vehicles, a development largely attributable to their exceptional properties [1,2]. Their low weight renders them ideal for lightweight construction, while their cost efficiency, attributable to reduced material usage and lower manufacturing and tooling expenses in injection molding, further enhances their appeal. Additionally, their high design flexibility enables the production of complex geometries, which is essential in many automotive applications. As Miller et al. [3] point out, sustainability is very important. Polypropylene (PP) is of particular relevance in this regard due to its recyclability, which offers significant benefits.

In addition, polymeric matrix materials are frequently reinforced with fillers, such as nanoparticles or minerals, with the objective of enhancing their mechanical and thermal properties while preserving stable process conditions. Furthermore, the impact on cost and processing parameters is negligible. Consequently, mineral- or nanoparticle-filled PP has become widely used in the automotive industry as an attractive alternative to fiber-reinforced PP, since fibers are comparatively more expensive, both as raw materials and in processing [4].

In the context of automotive exterior applications, the investigated PP grades are predominantly utilized in functional and semi-structural components, where the performance is governed by factors such as dimensional stability and vibration durability. For instance, PP without talc-filler is commonly used for ducting and air-guiding parts that are assembled in a constrained manner and therefore rely on sufficient elastic compliance. Conversely, talc-filled PP is extensively utilized in front and rear bumper fascia, and headlamp housings, where higher stiffness, reduced shrinkage, and lower warpage are imperative. These components are, as such, typically evaluated using coupled thermal and vibrational loading in climate–vibration durability protocols employed during the development of automotive technologies. Such evaluations generally encompass temperatures ranging from −40 °C to 100 °C and excitation frequencies spanning from a few to 100 Hz.

Accordingly, these conditions affect the thermal, mechanical, and viscoelastic properties of talc-reinforced PP, which have so far not been sufficiently examined experimentally in the automotive context.

Mechanical properties of talc-filled polypropylene The addition of talc can improve the mechanical properties and thermal stability of PP [5,6]. In most cases, the stiffness increases, whereas the incorporation of specific hybrid nanoparticles may even reduce the strength [5]. A similar conclusion was drawn by Lapcik et al. [7], who conducted mechanical tests on talc-free and talc-reinforced PP. Lapcik et al. [7] reported that the addition of talc increases strength, including tensile and flexural strength, while simultaneously reducing impact toughness, leading to increased brittleness of the talc–PP composite.

The properties of PP are also influenced by its semicrystalline structure, which varies with temperature and environmental conditions. Li et al. [8] explicitly reported that an increasing degree of crystallinity leads, for example, to a higher Young's modulus. The manufacturing process has the strongest influence on the degree of crystallinity. For example, both Zuidema et al. [9] and Hu et al. [10] experimentally demonstrated that higher cooling rates lead to significantly fewer crystalline regions, since these regions lack sufficient time to form. As a result, PP remains in a structurally non-equilibrated state. As stated by Gaspar-Cunha et al. [11], the cooling stage often accounts for 50–80 % of the total cycle time. This is particularly relevant in the automotive industry, where high production volumes demand high-speed processing, which in turn is typically associated with elevated cooling rates. Other processing parameters may also affect the degree of crystallinity. For instance, the mold temperature can exert a significant influence on the outcome, potentially resulting in a structurally non-equilibrated state of PP, as evidenced by [12]. This state, which has not fully relaxed toward structural equilibrium, gives rise to so-called post-crystallization effects [13]. According to Gahleitner et al. [13], these physical aging effects are more pronounced for polymers with a high amorphous fraction. However, Kościuszko et al. [12] also showed that annealing the samples aligns the physical properties regardless of the processing parameters applied during injection molding [12]. Talc also influences the degree of crystallinity. As demonstrated by Velasco et al. [14–16], talc particles act as nucleating agents in PP, thereby promoting faster crystallization and consequently leading to a higher final crystallinity.

Experimental characterization by dilatometry, dynamic mechanical analysis, and calorimetry Thermal expansion can induce internal stresses when constrained, which may result in warpage or shrinkage. This, in turn, can lead to tolerance deviations and surface defects such as sink marks. These effects are undesirable for both functional and aesthetic reasons and should be minimized as far as possible. However, there is a lack of studies in the literature that have investigated how the thermal expansion and the coefficients of thermal

expansion (CTE) of unfilled and talc-filled PP vary with temperature. The existing literature of research, which encompasses a considerably more limited temperature range, suggests that the incorporation of talc into PP typically results in a substantial reduction in the CTE [17–19]. Additionally, there is limited knowledge regarding the behavior of PP in a structurally non-equilibrated state and the effect of post-crystallization on its thermal expansion.

In addition to the thermal expansion, the viscoelastic behavior of PP is of great importance. Consequently, particular attention should be given to dynamic mechanical analysis (DMA) in the form of temperature-frequency sweeps, since these allow for a reliable assessment of the material's time-temperature-dependent behavior. Generally speaking, DMA facilitates the quantification of material parameters that can be incorporated into viscoelastic material models. These models find application in crash and structural simulations, as well as the assessment of the stiffness of polymeric connections, to determine their capacity to prevent failure or disengagement across service temperatures. In their investigations, Jourdan et al. [20] and Read [21] demonstrated the complex thermorheological response of pure PP. The two authors discussed in detail the relaxation and post-crystallization behavior as a function of temperature and frequency. In addition, experimental studies by Zhou et al. [18] and Bajsić et al. [17] found that the incorporation of fillers into the material resulted in an enhancement of its stiffness. However, very few studies address the behavior of PP under structurally non-equilibrated conditions, particularly the influence of post-crystallization and the degree of crystallinity on its viscoelastic response below the melting temperature, which is highly relevant for durability considerations in automotive applications.

Furthermore, differential scanning calorimetry (DSC) was employed to quantify the crystalline state of the PP materials. In semicrystalline polymers, crystallinity is not a fixed material constant but evolves with thermal history through processes such as post-crystallization and physical aging, which may be induced or accelerated by annealing treatments. Early work by Pae and Sauer [22] already indicated that thermal preconditioning can alter the degree of crystallinity, and Lima et al. [23] subsequently demonstrated a clear increase in crystallinity upon annealing. Since the crystalline fraction and the amorphous–crystalline morphology are known to influence thermal expansion and stiffness, DSC provides essential structural context for interpreting the dilatometric and DMA results. In addition, talc is known to affect crystallization kinetics and morphology, and DSC studies have reported increased crystallinity in talc-filled PP [14–16]. By assessing melting and crystallization behavior and evaluating the enthalpy of fusion, DSC enables a quantitative comparison of crystallinity between unconditioned and preconditioned states and between unfilled and talc-filled grades. This complementary information helps to link macroscopic changes in thermal expansion and damping to underlying, history-dependent microstructural development.

Outline and originality The manuscript first introduces the investigated PP grades (unfilled, 20 wt.% talc, and 40 wt.% talc) and motivates the material selection. Section 2 describes the experimental program and evaluation procedures for dilatometry (DIL), dynamic mechanical analysis (DMA), and differential scanning calorimetry (DSC). Section 3 presents and discusses the results with respect to the influence of thermal history and talc reinforcement on thermal expansion, viscoelastic response, and crystallinity, and highlights their relevance for automotive applications. Finally, the main findings are briefly discussed and summarized in Sect. 4.

The present work provides a consistent experimental characterization of how defined thermal states modify the temperature-dependent thermomechanical response of semicrystalline PP. The present study evaluates thermal expansion, viscoelastic mechanical behavior, and crystalline fraction for both unfilled and talc-filled grades. This joint evaluation enables to identify correlations between structural variations induced by prior thermal exposure to measurable changes in macroscopic response.

2 Materials and methods

2.1 Polypropylene with and without talc filler

For the experimental investigations, three PP-based materials were selected. The first material, SABIC®-PP-CX02-81 [24], was sourced from SABIC (Saudi Basic Industries Corporation). It is an unreinforced semicrystalline PP with UV stabilizer, primarily used in automotive interior applications. The second material, Hostacom-M2-U02, was obtained from LyondellBasell Industries [25]. This PP-based polymer is reinforced with 20 wt.% talc and is commonly applied in automotive interiors, air conditioning ducts, and exterior components such as front and rear attachments. The third material, Hostacom-M4-U02, also from LyondellBasell

Table 1 Material parameters obtained from published data sheets by the supplier

Material	Density (ISO-1183)	Tensile modulus (ISO-527)
SABIC®-PP-CX02-81	0.905 g/cm^3 [24]	1550 MPa [24]
Hostacom-M2-U02	1.040 g/cm^3 [25]	2600 MPa [25]
Hostacom-M4-U02	1.210 g/cm^3 [26]	4000 MPa [26]

Table 2 Test parameters for tests by DIL

Test parameter	Value
Temperature range	$\theta \in [-60, 110]$ °C
Maximum contact force	100 mN
Isothermal hold time	15 min
Temperature rate	2 K/min

Industries [26], is a PP-based polymer reinforced with 40 wt.% talc, offering significantly increased stiffness and strength. The densities and tensile moduli of the investigated materials are listed in Table 1.

The samples were manufactured by 4a engineering GmbH in Traboch, Austria. To ensure compatibility with the testing equipment, the geometries were precisely defined. For dilatometric analysis, rectangular samples were produced with dimensions of 2 mm in thickness, 10 mm in width, and 50 mm in length. For DMA, the samples measured 2 mm × 10 mm × 83 mm.

All samples were milled from injection molded plates made of the respective materials. Each plate had dimensions of 2 mm in thickness, 80 mm in width, and 120 mm in length. The longitudinal direction of each sample corresponds to the flow direction during injection molding. From each plate, three samples were prepared for dilatometric analysis and three for DMA testing.

Unless otherwise specified, all samples were preconditioned in a climate chamber at 20 °C and 50 % relative humidity. UV conditioning was not considered, as the materials contain UV stabilizers and, in the case of automotive exterior applications, are typically coated with paint.

The present study is constrained to the investigated commercial PP grades, which were selected based on their relevance for automotive applications rather than as a controlled material series with systematically varied talc content from a single supplier. Consequently, supplier-specific material characteristics may also contribute to the measured response. Moreover, the analysis did not consider molecular weight and molecular weight distribution, due to a lack of available data.

2.2 Dilatometry experiments

The dilatometric experiments were conducted using the DIL 402 Expedis® Select device by NETZSCH B.V. & Co. Holding KG. The system incorporates an electrically operated furnace into which the sample is placed. The measurements were conducted in a horizontal pushrod configuration. The sample is supported by two supports within the furnace. A sample end is then positioned against a fixed stop. The opposing end is contacted by the glass pushrod. In this instance, no clamping of the sample is applied but the sample is free to expand in the transverse directions, i.e. width and thickness. The pushrod contact force is maintained at a minimal level, limited to a maximum of 100 mN to ensure only nominal contact. Heating is facilitated by electrical means within the furnace, whereas the process of cooling is achieved by instreaming liquid nitrogen into the testing chamber. Furthermore, during the measurement procedure, the chamber is purged with gaseous nitrogen to prevent oxidation.

The calibration of the testing device is performed by using a certified reference material (fused silica) to ensure that systematic influences, such as the thermal expansion of the sample holder and pushrod, are accurately compensated. This reference sample is subjected to the exact same loading conditions as the actual samples. Dimensional changes are recorded as a function of temperature with high precision, using a contact-based displacement sensor. This allows for the reliable determination of material properties such as the CTE, the glass transition temperature, or phase transformations, depending on the material system and temperature range.

Table 2 summarizes the experimental settings applied in the dilatometric tests. The selected start and end temperatures slightly exceed the temperature range typically observed in automotive applications. The isothermal holding period ensures a uniform temperature distribution within the sample. The recorded data includes time, temperature, applied force, gas flow rate, and sample elongation. The deformation is evaluated in terms of engineering strain defined as

$$\varepsilon_{\text{eng}} = \frac{L - L_0}{L_0} = \frac{\Delta L}{L_0}, \tag{1}$$

where ΔL is the measured displacement of the glass pushrod. The initial length L_0 corresponds to the length of the sample at the beginning of the isothermal holding phase, specifically after the target start temperature of $-60\,^{\circ}\text{C}$ has been reached. From this point onward, the system starts recording the measurement data.

Based on the recorded data, the CTE can be determined in the postprocessing stage. Since the pushrod contact force is minimal, the measured deformation is attributed to free thermal expansion. The temperature-dependent coefficient of thermal expansion is therefore evaluated directly from the derivative of the measured engineering strain with respect to temperature as

$$\alpha(\theta) = \frac{\mathrm{d}}{\mathrm{d}\theta}\varepsilon_{\text{eng}}(\theta) = \frac{1}{L_0}\frac{\mathrm{d}L(\theta)}{\mathrm{d}\theta}. \tag{2}$$

For the numerical evaluation of this derivative, a first-order central difference scheme was employed. The derivative was not computed at the first and last data points. During the experiment, measurement data was recorded every 15 s. Given a heating rate of 2 K/min, this corresponds to a temperature increment of approximately 0.5 K between consecutive data points.

2.3 Dynamic mechanical analysis experiments

In this study, DMA of the samples is carried out using the GABO Eplexor® 500N testing device by NETZSCH B.V. & Co. Holding KG. Within a temperature-controlled chamber, the sample is clamped at both ends and loaded in uniaxial tension mode, accounting for small deformations. The DMA setup involves the application of a mechanical load to the sample [27], e.g. $\varepsilon(t)$. This load consists of a static preload ε_0 combined with a superimposed sinusoidal load of defined amplitude $\Delta\varepsilon$ and angular frequency $\omega = 2\pi f$, where f denotes the excitation frequency listed in Table 3, reading

$$\varepsilon(t) = \varepsilon_0 + \Delta\varepsilon \sin(\omega t). \tag{3}$$

The application of controlled strain enables the measurement of the stress response. Two distinct drive systems are utilized to generate the static and dynamic loads, respectively. The displacement-controlled spindle drive imposes the static preload, while the dynamic load is introduced via a force-controlled electromagnetic shaker. The deformation of the sample is monitored using both an inductive displacement sensor, which tracks the movement of the upper traverse, and a capacitive displacement sensor, which measures the motion of the shaker. The material response $\sigma(t)$ is then characterized by the stress amplitude and the phase shift between the applied cyclic load and the resulting cyclic stress [28], expressed as

$$\sigma(t) = \sigma_0 + \Delta\sigma \sin(\omega t + \delta), \tag{4}$$

where σ_0 is the mean stress and $\Delta\sigma$ is the stress amplitude. The ratio of stress amplitude to strain amplitude defines the magnitude of the complex modulus E^*, with $E^* = E' + iE''$, which characterizes the effective Young's modulus of the material. Due to the sinusoidal load, the complex modulus comprises an in-phase component, the storage modulus E', and an out-of-phase component, the loss modulus E''

$$E' = \frac{\Delta\sigma}{\Delta\varepsilon}\cos(\delta), \quad E'' = \frac{\Delta\sigma}{\Delta\varepsilon}\sin(\delta), \quad \tan\delta = \frac{E''}{E'}, \tag{5}$$

with the loss factor $\tan\delta$, where $\delta \in [0, \pi/2]$. In materials of a purely elastic nature, the following relationships hold true: $E^* = E'$, $E'' = 0$, and $\delta = 0$. In contrast, a purely viscous material exhibits $E^* = E''$, $E' = 0$, and $\delta = \pi/2$.

By subjecting the samples to varying temperature conditions, their thermomechanical behavior can be assessed. In the case of polymeric materials, the mechanical response is highly sensitive to both temperature and loading frequency.

The test parameters for the samples used in this study are listed in Table 3.

Table 3 Test parameters for temperature-frequency tests by DMA

Test parameter	Value
Static load	$\varepsilon_0 = 0.1\,\%$
Dynamic load	$\Delta\varepsilon = 0.05\,\%$
Frequency (7 log-spaced points)	$f \in [0.5, 50]\,\mathrm{Hz}$
Temperature	$\theta \in [-40, 120]\,^\circ\mathrm{C}$
Temperature increment and rate	$\Delta\theta = 5\,\mathrm{K}$ with $1\,\mathrm{K/min}$
Soak time after reaching target temperature	300 s

2.4 Differential scanning calorimetry experiments

Differential scanning calorimetry (DSC) is a thermoanalytical technique based on the principle of differential thermal analysis. It is widely used to characterize the thermal behavior of materials. In the context of a DSC experiment, samples are exposed to systematic heating and cooling cycles. The mass-specific heat flow rate $\dot{q}(\theta)$ is measured as a function of temperature using a differential measurement principle. In the present study, a Mettler Toledo DSC 1 operated in heat-flux mode was employed. In this configuration, the PP sample and an inert reference are placed in the same measurement chamber, and the instrument measures the temperature difference between the sample and reference platforms. Endothermic and exothermic processes, including melting and crystallization, manifest as deviations in the heat-flow signal. Detailed theoretical derivations can be found in the works of Wunderlich [29], Höhne et al. [30], and Ehrenstein et al. [31].

By employing the mass-specific melting enthalpy Δh_m, which effectively represents the heat required to melt the polymer, the degree of crystallinity of the semicrystalline PP can be determined by

$$\chi_\mathrm{c} = \frac{\Delta h_\mathrm{m}}{\Delta h_\mathrm{m}^{100}} \cdot 100\,\%, \tag{6}$$

with $\Delta h_\mathrm{m}^{100}$ denoting the mass-specific melting enthalpy of a fully crystalline PP [29]. For the talc-filled Hostacom grades, the measured melting enthalpy was therefore normalized to the effective PP mass, $m_\mathrm{PP} = w_\mathrm{PP}\, m$, with w_PP given by 0.8 for 20 wt% talc, and 0.6 for 40 wt% talc. Thereby, Δh_m and χ_c refer to the polymer phase rather than the total sample mass. In the present study, $\Delta h_\mathrm{m}^{100} = 170\,\mathrm{J/g}$ is used according to Lanyi et al. [32].

The DSC measurements were conducted over a temperature range of $\theta \in [-80, 250]\,^\circ\mathrm{C}$ at a constant temperature rate of 10 K/min, consistent with ISO 11357-1 [33].

3 Results

3.1 Dilatometry experiments

3.1.1 Coefficients of thermal expansion results

Samples extracted from the same plate exhibited low variability in the measured response. As indicated by the DIL measurements, equivalent results were obtained for samples extracted from separate plates of SABIC®-PP-CX02-81. As illustrated in Fig. 9 in the Appendix, the mean values and standard deviations of three SABIC®-PP-CX02-81 samples tested under comparable testing conditions are presented, indicating no systematic differences that exceed the experimental scatter. Despite the fact that the Hostacom samples are talc-filled and therefore not homogeneous on the microscale, the reproducibility of the measured macroscopic response indicates a comparable level of material consistency for these material systems.

The subsequent figures depict the CTE as a function of the temperature. The legend distinguishes between four test conditions that are summarized in Table 4.

The as-received state was included because it represents the technically relevant delivery condition of the investigated commercial grades, although its prior thermomechanical history is not fully known. This condition is relevant from an application perspective, since comparable material states may also occur in automotive components prior to subsequent environmental exposure during service. Tests 2 and 3 were used to assess changes after a first thermal exposure and subsequent storage, respectively. Test 4 provides a defined thermal preconditioning state and therefore serves as a controlled reference for evaluating thermal-history effects.

Table 4 Conditions of test samples used for DIL and DMA experiments

Test no.	Statement on condition
Test 1	as-received, unaltered sample
Test 2	experiments conducted within 24 h after testing Test 1
Test 3	experiments conducted more than one month after Test 2
Test 4	experiments with samples preconditioned at 100 °C for minimum 36 h

The preconditioning temperature of 100 °C was selected as a defined upper-temperature exposure within the service-relevant range considered for automotive applications, while remaining below the melting range of PP, cf. [34]. The duration of at least 36 h was chosen as a reproducible multi-day exposure that exceeds the time required for thermal equilibration and allows thermally activated structural stabilization without melting the material.

*SABIC®-PP-CX02-81*An overview of the thermal expansion behavior is provided in Fig. 1 for the material SABIC®-PP-CX02-81. In Test 1, the CTE increases nearly linearly from −50 °C up to about 20 °C. It then rises sharply, reaching a local maximum near 50 °C. This is followed by a distinct drop in CTE between 60 °C and 80 °C, forming a noticeable dip in the curve. For temperatures higher than 90 °C, the curve begins to rise again.

The behavior in Test 2 initially follows a comparable pattern as Test 1, particularly up to approximately −20 °C. From there, however, it increases more strongly up to around 0 °C. Beyond this point, the curve flattens slightly but continues to rise in a nearly linear fashion. As a result, the progression appears more monotonic and consistent compared to Test 1. Around 40 °C, the curve of Test 2 intersects with that of Test 1 and continues its nearly linear increase throughout the remaining temperature range.

Test 3, by comparison, shows consistent tendencies at lower temperatures. Notably, from approximately −20 °C onward, the curve mirrors Test 1, corresponding to the initial, unaltered state of the sample. The same tendency persists up to the peak at around 50 °C. Subsequently, the curve slightly decreases and eventually converges with the progression recorded in Test 2 at approximately 90 °C.

In Test 4, the CTE matches Tests 1 and 3 up to about 40 °C, follows Test 2 between 40 and 60 °C, and remains higher than Test 1 above 60 °C. This behavior may be attributed to the extended annealing treatment, which likely relaxed the sample and reduced its overall expansion. The progression can be regarded as a combination of the previous tests. Up to approximately 40 °C, the curve resembles that of Tests 1 and 3. Thereafter, the increase levels off and no peak is observed at around 50 °C, in contrast to Tests 1 and 3, while the response is very similar to Test 2. At approximately 80 °C, the curve deviates from this trend, exhibiting an abrupt increase and a kink near 100 °C, which corresponds to the maximum temperature applied during thermal preconditioning. The curve then converges with those of Tests 2 and 3 at around 110 °C. This behavior may be associated with the melting memory effect, which, according to Cho et al. [35], indicates that the structure of PP depends on the melting temperature and hold time, thereby influencing its crystallization behavior during cooling as well as its phase transformation behavior during heating. In the present case, the CTE response appears to retain a memory at the last maximum temperature experienced by the sample.

In the context of automotive exterior components, the CTE results underscore the notion that the dimensional response can be history-dependent, a phenomenon that is particularly evident during the initial thermal exposure following processing or storage.

These observations are particularly relevant for automotive exterior components assembled under geometric constraints (e.g., clips, screws, or guided interfaces), where thermal expansion cannot be accommodated freely and may lead to stress build-up, tolerance shifts, and warpage. A comparison of unconditioned and preconditioned states reveals that thermal cycling renders the CTE response more monotonic and reproducible, thereby enhancing dimensional stability. Consequently, thermal history should be considered not only during processing, but also during storage and early-life thermal exposure.

Hostacom-M2-U02 The thermal expansion characteristics of Hostacom-M2-U02 are presented in Fig. 2. The qualitative characteristics broadly resemble those of SABIC®-PP-CX02-81. Test 1 shows similar characteristic features, including an additional plateau up to about −20 °C, followed by a gradual increase up to around 40 °C. A sharp rise leads to a maximum at 50 °C, which is followed by a pronounced drop between 60 and 80 °C. The local minimum occurs at approximately 90 °C, after which the curve rises again. In contrast to

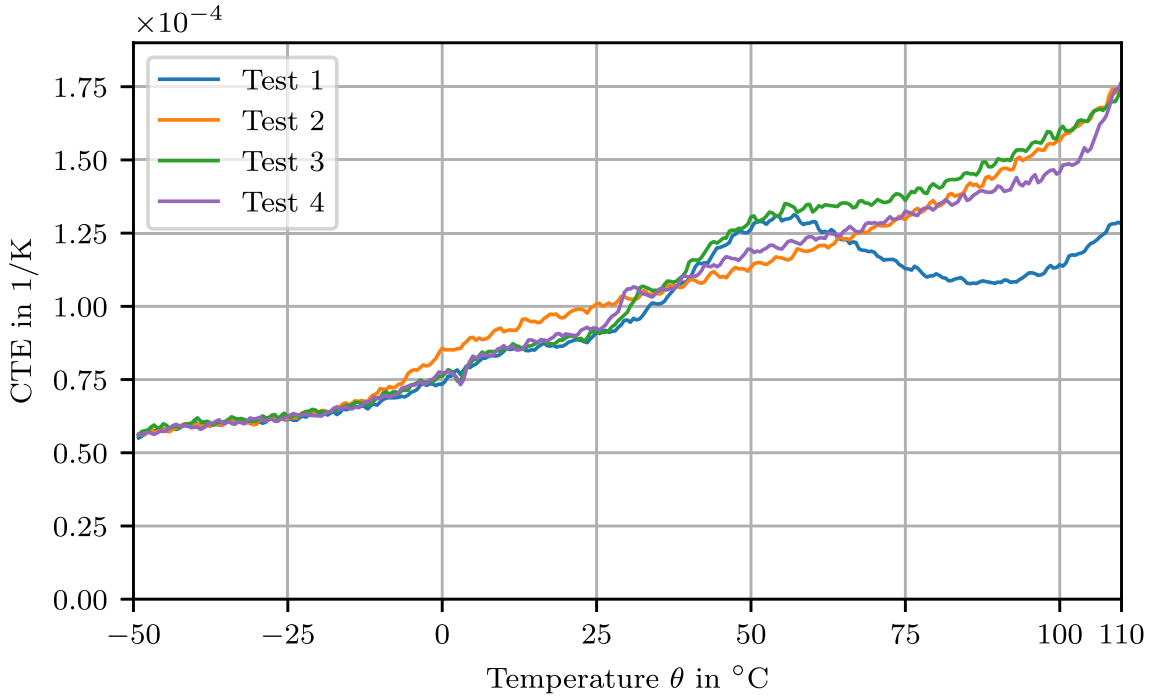

Fig. 1 Thermal expansion of SABIC®-PP-CX02-81: CTE, cf. Equation 2, shows regions of nearly constant expansion, peaks, and dips indicative of structural or phase transitions. Differences between tests reflect sample treatment, annealing, and the melting memory effect. Test 1: as-received; Test 2: <24 h after Test 1; Test 3: months later; Test 4: preconditioned at 100 °C for 36 h

SABIC®-PP-CX02-81 distinct variations are apparent at lower temperatures, where the curve is significantly flatter, particularly in the range between −50 and −20 °C. Additionally, the CTE values are clearly lower at low temperatures compared to SABIC®-PP-CX02-81, but they converge to nearly identical levels at higher temperatures.

Tests 2 and 3 demonstrate trends analogous to those observed for SABIC®-PP-CX02-81. Test 2 shows a nearly identical temperature-dependent progression, including the initial plateau, subsequent increase, and gradual linear rise at higher temperatures. In Test 3, the peak at approximately 50 °C is more pronounced, followed by convergence with Test 2 at elevated temperatures. The qualitative behavior exhibited by Test 4 is analogous to that observed in SABIC®-PP-CX02-81. However, Test 4 demonstrated a closer agreement with Test 2 than it was observed for the previous material.

The reduced CTE of Hostacom-M2-U02, particularly at sub-zero temperatures, is consistent with its high talc content, whereas the values at around 110 °C finally reach the same quantitative levels as those of SABIC®-PP-CX02-81.

Hostacom-M4-U02 In Fig. 3, the CTE response of Hostacom-M4-U02 is displayed. The qualitative response in Tests 1 and 2 appears to be consistent with that of both SABIC®-PP-CX02-81 and Hostacom-M2-U02.

However, quantitative variations in the temperature levels have been observed. At low temperatures, the CTE values are marginally lower than those of Hostacom-M2-U02. At elevated temperatures, the curve shows a less pronounced increase, which is likely attributed to the even higher talc content in Hostacom-M4-U02.

Slightly larger discrepancies are evident in comparison to the other materials for Test 3. The progression is qualitatively similar to Hostacom-M2-U02 up to the peak at approximately 50 °C, which is again higher and more pronounced. After this point, the CTE decreases and also converges toward Test 2, although the curves never fully meet.

With regard to the impact of talc incorporation, the CTE curves of Hostacom-M2-U02 and Hostacom-M4-U02 have been shown to reduce the apparent CTE. This property assists in preserving gap-and-flush requirements, i.e., maintaining specified clearances and flush alignment between adjacent exterior components, and in mitigating thermally induced distortion. In constrained assemblies, dimensional stability is contingent on both thermal strain and stiffness. Given that talc also increases stiffness, talc-filled grades may contribute

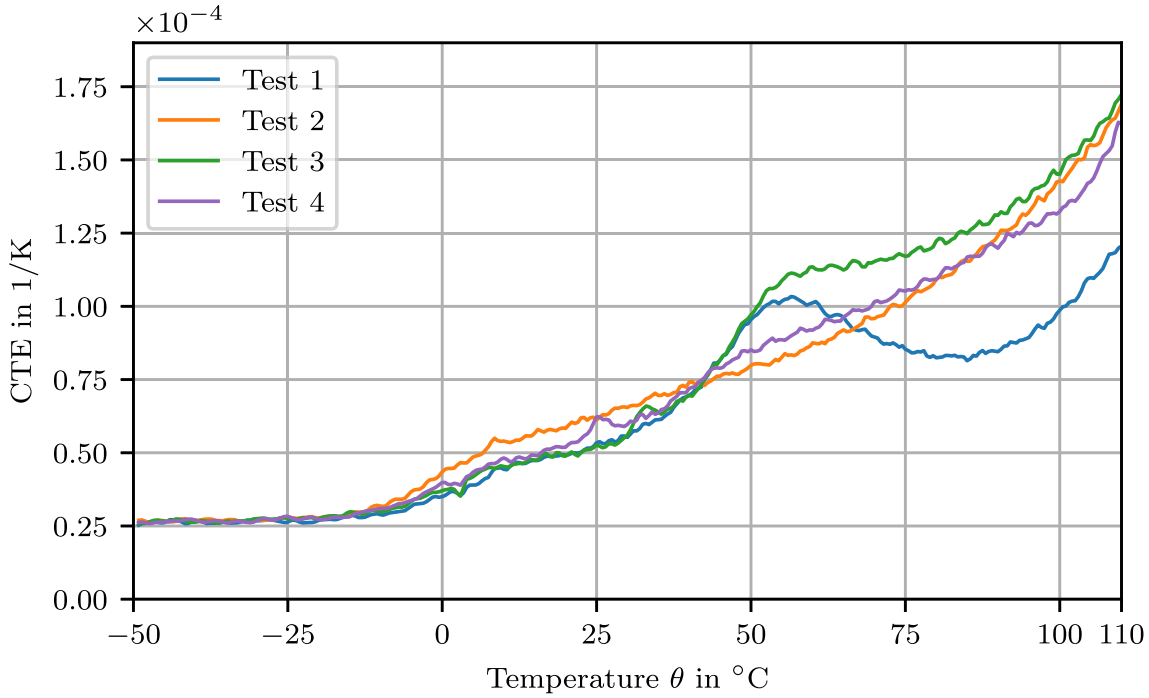

Fig. 2 Thermal expansion of Hostacom-M2-U02: CTE, cf. Equation 2, shows similar trends to SABIC®-PP-CX02-81, with nearly constant expansion at low temperatures, peaks around 50 °C, and a dip between 60 °C–90 °C. Lower CTE at sub-zero temperatures reflects high talc content, while convergence at higher temperatures is observed. Test 1: as-received; Test 2: < 24 h after Test 1; Test 3: months later; Test 4: preconditioned at 100 °C for 36 h

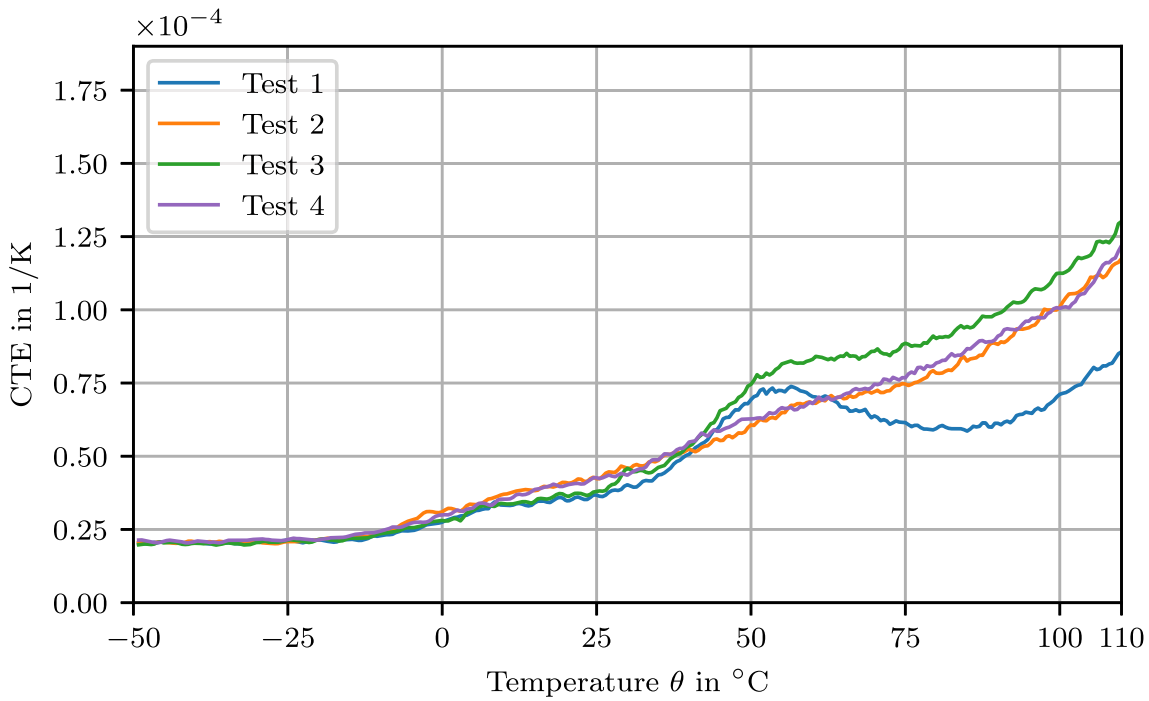

Fig. 3 Thermal expansion of Hostacom-M4-U02: CTE, cf. Equation 2, displays a pronounced initial increase at low temperatures, followed by a decrease and subsequent increase. The preconditioned sample exhibits a response similar to Test 2, indicating that the structural state achieved after thermal treatment is stabilized. Furthermore, the higher talc content is associated with lower CTE values compared to Hostacom-M2-U02. Test 1: as-received; Test 2: <24 h after Test 1; Test 3: months later; Test 4: preconditioned at 100 °C for 36 h.

to enhanced geometric stability in applications where thermal deformation is constrained. Conversely, unfilled PP may be advantageous when elastic compliance is required to accommodate tight mounts.

3.1.2 Interval-based comparison of coefficients of thermal expansion

As illustrated in Fig. 4, the arithmetic mean of all discrete CTE data points within two temperature intervals was calculated to obtain representative CTE values for the lower and higher temperature regimes. For a temperature interval $[\theta_a, \theta_b]$, the interval-averaged CTE is defined as

$$\bar{\alpha}_{\theta_a-\theta_b} = \frac{1}{N_{\theta_a-\theta_b}} \sum_{\theta_i \in [\theta_a,\theta_b]} \alpha(\theta_i), \tag{7}$$

where $\alpha(\theta_i)$ denotes the discrete CTE value evaluated at temperature θ_i and $N_{\theta_a-\theta_b}$ is the number of data points within the respective interval. No monotonicity assumption is made in this evaluation. Local peaks, dips, and scatter within the selected interval contribute directly to the arithmetic mean. The interval averages should therefore be interpreted as compact descriptors of the effective CTE level in the respective temperature ranges rather than as fitted material constants.

The temperature intervals ranging from 0 to 40 °C and from 40 to 100 °C were selected to differentiate between the quasi-linear expansion region below the pronounced structural transition around 50 °C and the regime in which non-monotonic features are observed. In order to quantify the temperature sensitivity of the effective thermal expansion independently of the absolute CTE level, the relative deviation

$$e_{\bar{\alpha},\mathrm{rel}} = \frac{\bar{\alpha}_{40\text{-}100} - \bar{\alpha}_{0\text{-}40}}{\bar{\alpha}_{0\text{-}40}} \times 100\,\% \tag{8}$$

is defined and summarized in Table 5. Normalizing with respect to $\bar{\alpha}_{0\text{-}40}$ facilitates direct comparison between unfilled and talc-filled materials despite their divergent absolute expansion coefficients. The resulting scalar measure reflects the relative increase in expansion behavior at elevated temperatures and thus serves as an indicator of the structural sensitivity of the material to thermal activation.

Across all materials and test conditions, the interval mean in the higher-temperature range exceeds that in the lower-temperature range, i.e., $\bar{\alpha}_{40\text{-}100} > \bar{\alpha}_{0\text{-}40}$ (Fig. 4), reflecting the overall increase in the CTE level with temperature. For the unfilled SABIC®-PP-CX02-81 grade, the relative deviation between both interval means is lowest in Tests 1 and 2 (31.3−32.6 %) and highest after aging (Test 3, 50.4 %). The comparatively slight deviation observed in Test 1 is influenced by the pronounced non-monotonic CTE drop around 60 and 80 °C. This drop reduces the mean in the 40 to 100 °C interval.

The addition of talc results in a substantial decrease in the absolute CTE level across both intervals (Fig. 4). A further reduction in CTE is observed for the Hostacom-M4-U02 in comparison to the Hostacom-M2-U02 material. Despite the reduced CTE level, the relative deviation is substantially larger for the talc-filled materials (Table 5), indicating an enhanced sensitivity of the effective expansion response to thermal activation. In Test 3, the relative deviation exceeds 120 % for both talc-filled grades, indicating that the temperature-induced increase in CTE is more than twice the low-temperature reference value. For both talc-filled grades, the increased deviation after aging suggests enhanced structural rearrangement or post-crystallization effects activated during reheating.

The interval-based evaluation confirms that, irrespective of conditioning state, the effective CTE is consistently higher in the upper temperature range than in the lower one. While talc incorporation has been demonstrated to reduce the overall expansion level, it has also been shown to amplify the relative temperature sensitivity of the response, particularly after aging. Therefore, the quantitative comparison indicates that filler addition and thermal history modify not only the magnitude but also the temperature dependence of the effective expansion behavior within the investigated range.

The DIL measurements demonstrate a discernible correlation between the CTE response and the thermal history. The peak–dip feature observed in the unconditioned state (Test 1) indicates a thermally activated structural rearrangement during heating, consistent with processes commonly associated with post-crystallization in semicrystalline PP. Prior thermal exposure (Tests 2 and 4) results in a predominantly monotonic CTE progression, suggesting a more stabilized material state. Following an extended period (Test 3), the reemergence of enhanced non-monotonic characteristics suggests a partial restoration of a structurally non-equilibrated condition. These interpretations are consistent with thermally activated structural processes. However, they cannot be verified directly by dilatometry alone.

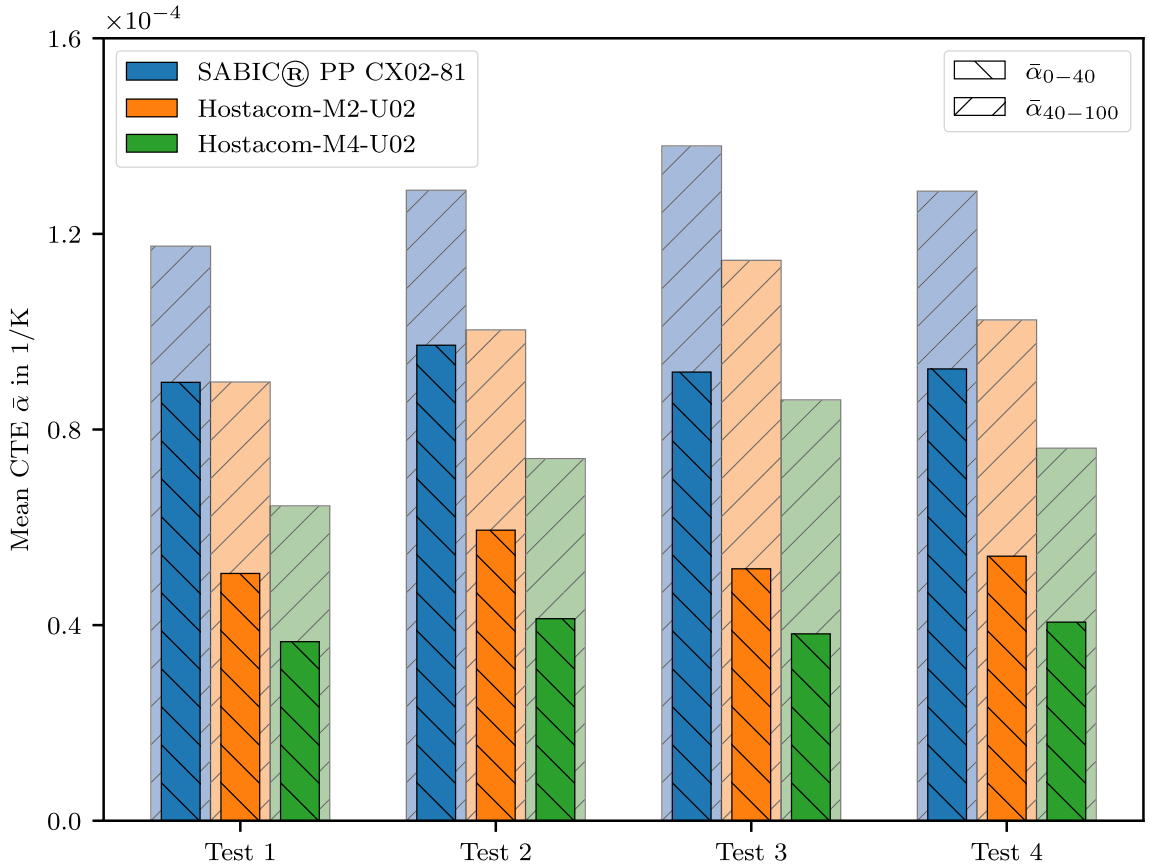

Fig. 4 Interval-averaged CTE for three polypropylene grades SABIC®-PP-CX02-81, Hostacom-M2-U02 and Hostacom-M4-U02 across four test conditions

Table 5 Relative deviation, $(\bar{\alpha}_{40\text{-}100} - \bar{\alpha}_{0\text{-}40})/\bar{\alpha}_{0\text{-}40} \times 100\,\%$, between the interval means $\bar{\alpha}_{0\text{-}40}$ and $\bar{\alpha}_{40\text{-}100}$ for all materials

Test no.	SABIC®-PP-CX02-81	Hostacom-M2-U02	Hostacom-M4-U02
Test 1	31.3 %	77.4 %	75.8 %
Test 2	32.6 %	68.9 %	79.3 %
Test 3	50.4 %	122 %	125 %
Test 4	39.3 %	89.3 %	87.6 %

From an engineering applications perspective, the interval specified in Fig. 4 and Table 5 suggests the utilization of a two-segment representation of the CTE over the designated temperature range. This approach diverges from the conventional practice of employing a single, constant CTE value, which is commonly applied in structural automotive simulations.

3.2 Temperature-frequency sweeps by dynamic mechanical analysis

3.2.1 Unconditioned dynamic mechanical analysis experiments

Storage modulus In Fig. 5 the storage modulus E' for all three material systems is plotted over the temperature θ. For all materials, E' decreases with increasing temperature and exhibits a distinctly non-linear, sigmoidal trend with an inflection point around $\theta \approx 0\,°\text{C}$. As expected, increasing frequency leads to an increase in the storage modulus. The curves are generally closely spaced, with the frequency-induced separation becoming more pronounced near the inflection region.

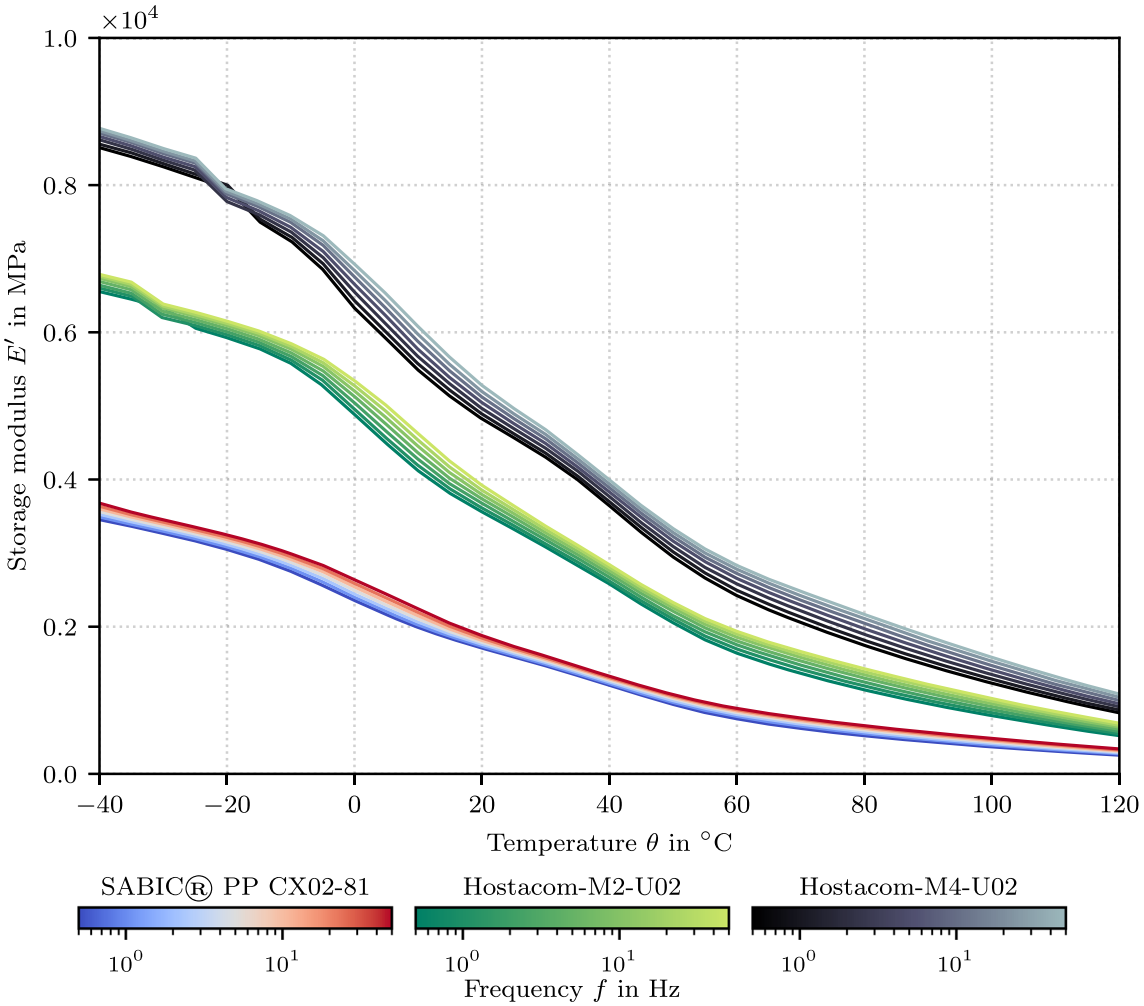

Fig. 5 Storage modulus E' for SABIC®-PP-CX02-81, Hostacom-M2-U02, and Hostacom-M4-U02, cf. Eq. 5, over θ for different frequencies. For all materials, E' decreases nonlinearly with increasing temperature, while higher frequencies yield higher E'. Across all three materials, E' suggests an inflection point around $\theta \approx 0\,°C$. Compared to SABIC®-PP-CX02-81, the talc-filled grades exhibit elevated modulus levels and a more pronounced frequency-induced separation; Hostacom-M4-U02 shows the highest E' across the entire range, with the largest differences at low temperatures

The incorporation of talc into the Hostacom-M2-U02 and Hostacom-M4-U02 samples led to an elevation in the modulus level in comparison to the SABIC®-PP-CX02-81 sample, a phenomenon that was most evident at low temperatures. This stiffening trend persisted throughout the entire temperature range, as evidenced by the highest E' values recorded. With respect to absolute values, the stiffness differences are most pronounced at low temperatures. Toward higher temperatures, the E' curves converge, such that the apparent separation between the grades decreases.

Loss factor Figure 6 provides an overview of the loss factor response of the three material systems, considering the effects of temperature and frequency. For all materials, $\tan\delta$ increases with temperature, indicating a progressively more dissipative and less elastic response at elevated temperatures. A pronounced local maximum is evident, occurring around 5–10 °C for all grades. According to [36], at least five common methods exist for determining the glass transition temperature θ_g. In this study, the glass transition is identified using the maximum of the loss factor, cf. Ferry [37, Chapter 2 A.9]. Thus, for this study, the above mentioned temperature range is consistent with the glass transition temperature θ_g of PP, as reported by Tajvidi et al. [38]. A slight frequency dependence is observed, with the θ_g-related maximum shifting to higher temperatures as frequency increases. The peak position remains comparable across materials, indicating that the predominant segmental relaxation associated with θ_g is not shifted by the filler. The peak magnitude is also largely similar, with

only Hostacom-M4-U02 showing a slightly reduced maximum. This finding suggests a moderation of the glass-transition-related dissipation with increasing talc content.

Following the maximum, tan δ decreases within the temperature range of approximately 20–35 °C. The position of the minimum is shifted toward higher temperatures with increasing frequency. This local minimum indicates a temperature range with reduced internal friction. With increasing temperatures, tan δ rises again. For SABIC®-PP-CX02-81, an additional, frequency-dependent maximum is clearly visible around 90–100 °C at low frequencies and shifts toward higher temperatures with increasing frequency. The location and character of this feature are consistent with the so-called α^*-relaxation [27], which describes a process that has been interpreted in the literature as the diffusion of defects within the crystalline phase [20]. Furthermore, Jourdan et al. [20] observed that the amorphous regions surrounding the crystalline domains facilitate and accelerate this defect diffusion. Conversely, for the talc-filled grades this corresponding high-temperature feature is shifted toward higher temperatures and is therefore only partially captured within the plotted range. Consequently, its presence is primarily notable at the lowest frequencies. This finding suggests a potential influence of talc on the so-called high-temperature defect-diffusion mechanism [20] associated with the α^*-relaxation. Furthermore, at temperatures ranging from approximately 50–60 °C, the absolute level of tan δ exhibits a systematic increase with increasing talc content. In this context, Hostacom-M4-U02 exhibits the highest loss factor, followed by Hostacom-M2-U02. In contrast, SABIC®-PP-CX02-81 maintains the lowest level, indicating that elevated temperatures and increased talc content promote dissipative behavior for small deformations.

From an engineering perspective, the high-temperature α^*-relaxation is not considered as a standalone design parameter. However, it provides an indicator for changes in the viscoelastic response at elevated temperatures. This is relevant for automotive exterior components exposed to high ambient temperatures and solar radiation, particularly for dark-painted parts, where surface and component temperatures may approach the upper range of the investigated service conditions. In this regime, changes in damping and stiffness may affect preload retention, dimensional stability, and vibration response of constrained assemblies.

3.2.2 Preconditioned dynamic mechanical analysis experiments

Loss factors As illustrated in Fig. 7, the loss factor, denoted by tan δ, of unconditioned and preconditioned samples is compared at a frequency of 5 Hz. In essence, the impact of preconditioning is predominantly characterized by its effect on the damping magnitude. Preconditioning primarily alters the damping level, inducing a systematic offset in tan δ over a broad temperature range, and the curves consistently intersect near 35 °C. The intersection occurs in the transition region between the glass transition-related loss peak and the subsequent high-temperature increase in tan δ, where the influence of preconditioning changes from an increase to a decrease in the loss factor.

In the lower-temperature range below this intersection region, the preconditioned samples exhibit elevated tan δ values, which are consistent with the relative deviations presented in Fig. 7 and summarized in Table 6. The enhancement in the glass-transition-related maximum is approximately 24 % for SABIC®-PP-CX02-81, 35 % for Hostacom-M2-U02, and 18 % for Hostacom-M4-U02. From an automotive point of view, this trend may prove advantageous in terms of resonance mitigation and rattle suppression during cold operation.

Above the intersection region at 35 °C, the trend is reversed. Specifically, preconditioning has been shown to result in a reduction in the loss factor, which indicates a response characterized by reduced dissipation. This behavior is documented in, e.g., Gahleitner et al. [39] and Fiebig et al. [40]. The enhanced stiffness retention at elevated service temperatures is advantageous in minimizing softening-induced loss of preload or geometric stability under prolonged thermal exposure.

While thermal preconditioning modifies the magnitude of the viscoelastic response, the glass transition temperature and the high-temperature α^*-relaxation remain largely unaffected. The alterations manifest predominantly in the stiffness and damping behavior of the material system, rather than in a shift of the transition temperatures.

3.3 Differential scanning calorimetry experiments

3.3.1 Overview of differential scanning calorimetry results

The DSC results (cf. Fig. 8) reveal a single dominant endothermic melting peak for all material systems during the first heating cycle. The peak temperature remains essentially unchanged after preconditioning, whereas

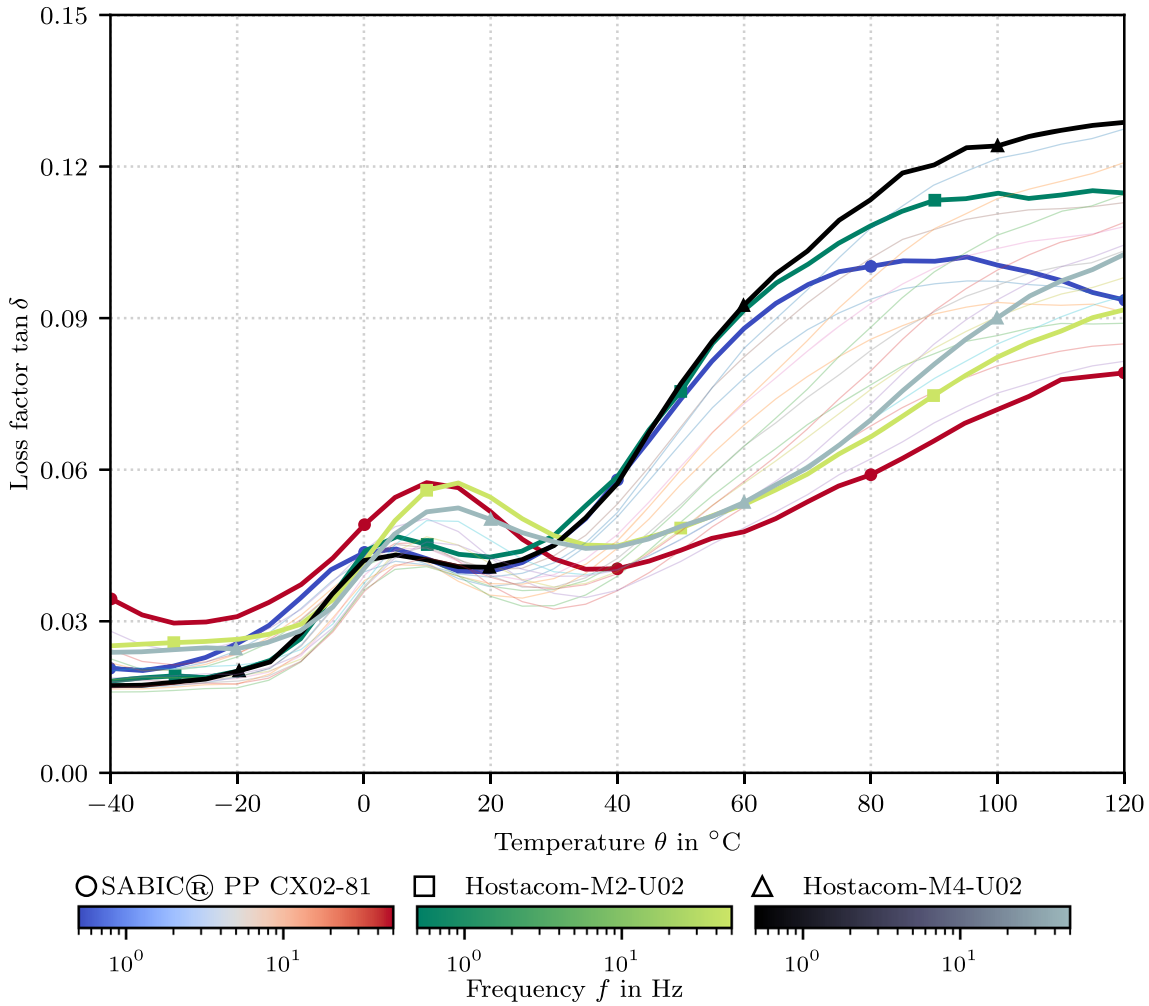

Fig. 6 Loss factor $\tan\delta$ for SABIC®-PP-CX02-81, Hostacom-M2-U02, and Hostacom-M4-U02, cf. Eq. 5, over θ for varying frequencies. All three materials exhibit a primary maximum around $\theta \approx 5$ to 10 °C, consistent with θ_g, followed by a local minimum at $\theta \approx 20$ to 35 °C. At higher temperatures, $\tan\delta$ increases with a pronounced frequency dependence; compared to SABIC®-PP-CX02-81, the talc-filled grades show a shift of the α^*-relaxation to higher temperatures and an overall higher loss level, most pronounced for Hostacom-M4-U02

Table 6 Comparison between preconditioned and unconditioned PP-samples depicted at $f \approx 5$ Hz

Sample	SABIC®-PP-CX02-81		Hostacom-M2-U02		Hostacom-M4-U02	
	$\tan\delta_{\theta_g}$	$\tan\delta_{T_{min}}$	$\tan\delta_{\theta_g}$	$\tan\delta_{T_{min}}$	$\tan\delta_{\theta_g}$	$\tan\delta_{T_{min}}$
Unconditioned	0.0435	0.0330	0.0448	0.0367	0.0426	0.0364
Preconditioned	0.0539	0.0340	0.0606	0.0388	0.0503	0.0361
Relative deviation	23.87 %	2.97 %	35.33 %	5.75 %	18.04 %	0.71 %

the peak area increases, consistent with the higher melting enthalpy values reported in Table 7. Since the melting enthalpy of the first heating cycle reflects the crystalline fraction present in the initial material state, these results indicate an increase in crystallinity following thermal treatment. In contrast, the crystallization enthalpy measured during controlled cooling exhibits no systematic differences between conditioning states, suggesting comparable crystallization behavior under identical DSC cooling conditions.

Quantitatively, thermal preconditioning increases the crystalline fraction by approximately 6.6 % for SABIC®-PP-CX02-81 and for Hostacom-M2-U02, and by 3.9 % for Hostacom-M4-U02. These changes in crystalline content are consistent with the modifications observed in the dilatometric and dynamic mechan-

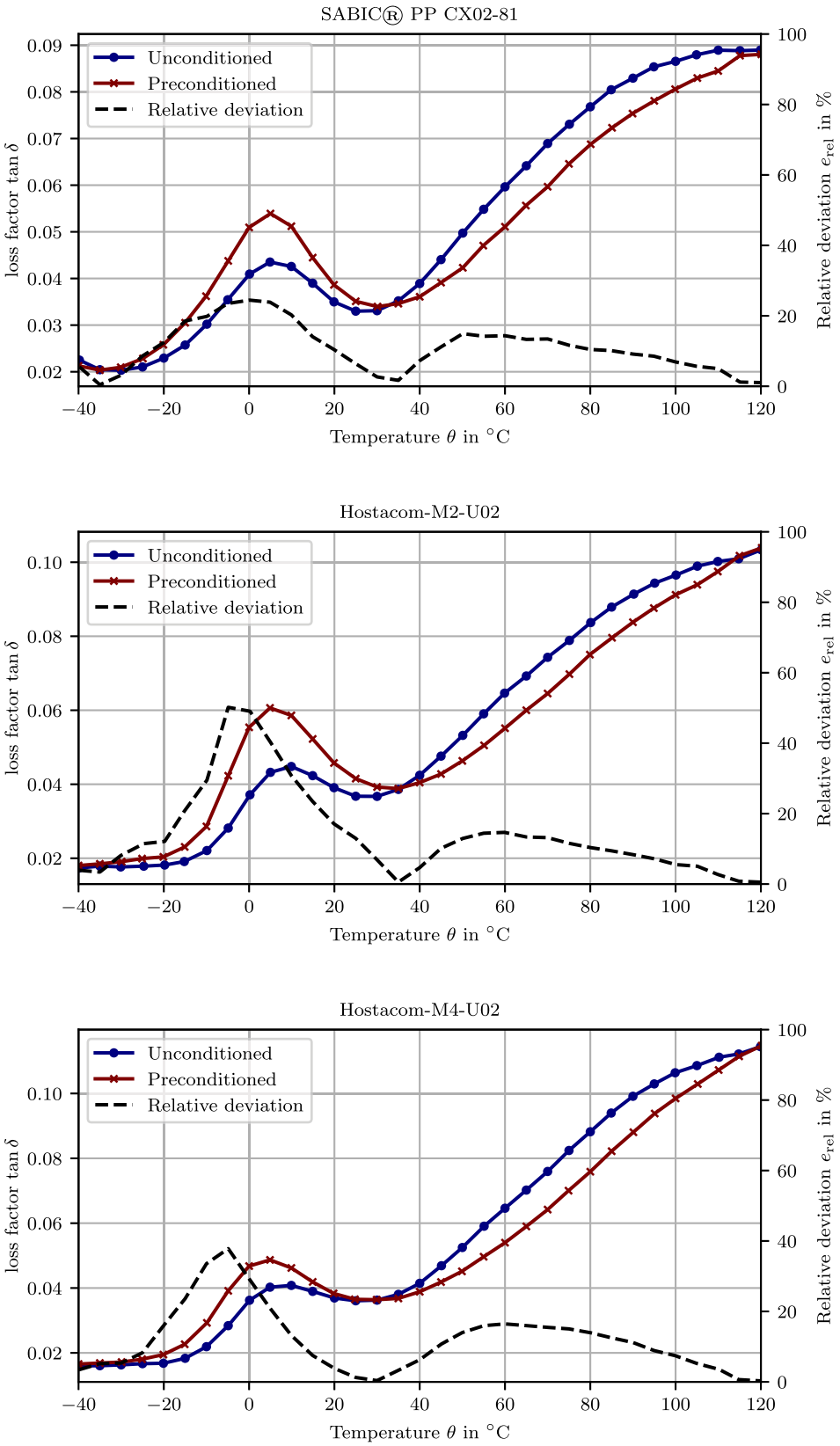

Fig. 7 Loss factors, cf. Equation 5, and their relative deviations for unconditioned and preconditioned samples at 5 Hz. Below 35 °C, preconditioning increases the loss factor tan δ, whereas above 35 °C it decreases tan δ compared to the unconditioned samples. Relative deviations are largest in the low-temperature region and decrease non-monotonically at higher temperatures. No shift in θ_g and α^*-relaxation is observed

Table 7 Integration limits and adjusted mass m_{PP} used to determine the mass-specific enthalpy of melting Δh_m and the degree of crystallinity χ_c for all materials in the unconditioned and preconditioned states

Values	SABIC®-PP-CX02-81		Hostacom-M2-U02		Hostacom-M4-U02	
	Uncond.	Precond.	Uncond.	Precond.	Uncond.	Precond.
m_{PP}	4.091 mg	5.113 mg	6.256 mg	7.097 mg	6.690 mg	5.271 mg
Δh_m	80.68 J/g	92 J/g	91.64 J/g	102.80 J/g	95.69 J/g	102.38 J/g
χ_c	47.46 %	54.12 %	53.91 %	60.47 %	56.29 %	60.22 %

For the talc-filled Hostacom grades, Δh_m was normalized to the effective PP mass as described in Sect. 2.4

ical measurements, where a more monotonic CTE evolution and altered stiffness and damping levels were identified after thermal treatment.

Furthermore, the talc-filled grades exhibit higher crystallinity than the unfilled material in both conditioning states, in agreement with the well-documented nucleating effect of talc, see Velasco et al. [14] and Castillo and Barbosa [15].

While DSC quantifies the crystalline fraction, it does not directly resolve changes in amorphous-phase segmental mobility. Thus, the structural interpretation remains indirect. Therefore, the observed changes in crystallinity are interpreted as correlated with the changes in CTE, stiffness, and damping.

4 Summary and conclusion

This study combines dilatometry (DIL), dynamic mechanical analysis (DMA), and differential scanning calorimetry (DSC) to quantify how thermal history and talc reinforcement affect thermal expansion, viscoelastic response, and crystallinity of polypropylene (PP) under service-relevant conditions in an automotive context.

Key conclusions

- *Thermal preconditioning stabilizes the thermal-expansion response:* DIL shows a more monotonic temperature dependence of the CTE after preconditioning, with a suppression of pronounced non-monotonic features observed in the unconditioned state.
- *Preconditioning primarily changes the magnitude, not the characteristic temperatures, of the DMA response:* DMA identifies two characteristic features in the loss-factor response (glass transition at low temperatures and the high-temperature α^*-relaxation). Thermal preconditioning mainly alters stiffness and, in particular, damping levels, while the temperature positions of both glass transition and α^*-relaxation remain largely unchanged.
- *DSC provides a consistent structural trend:* DSC confirms an increased crystalline fraction after thermal preconditioning. This trend provides structural context for the observed modifications in CTE as well as stiffness and damping levels, while no direct causal relationship is inferred from DSC alone.
- *Talc reinforcement shifts levels and high-temperature α^*-relaxation:* Compared to the unfilled grade, talc incorporation reduces the absolute CTE level and increases stiffness and crystalline fractions. In addition, talc affects the high-temperature α^*-relaxation, whereas the glass transition temperature remains essentially unaffected.

For constrained automotive exterior assemblies (e.g., clips, screws, or guided interfaces), the observed history dependence of the CTE implies that thermal cycling and early-life exposure can directly affect dimensional stability, tolerance shifts, and warpage. In this context, the more monotonic and reproducible CTE response after thermal preconditioning indicates a practical route to reduce scatter and improve robustness. Moreover, the combined DIL/DMA trends suggest that talc-filled grades can enhance geometric stability through reduced thermal strain and increased stiffness, whereas unfilled PP may remain advantageous when elastic compliance is required for assembly and in-service accommodation.

The experimental approach presented herein provides a structured dataset for correlating thermal expansion, viscoelastic response, and crystalline fraction in PP grades relevant for automotive applications. However, the present study does not resolve the detailed microstructural mechanisms governing the observed changes. In addition to talc content and thermal history, supplier- and grade-specific characteristics may also contribute to the measured response. The reported trends should therefore be interpreted as an indication of history sensitivity rather than a direct identification of the underlying morphology evolution.

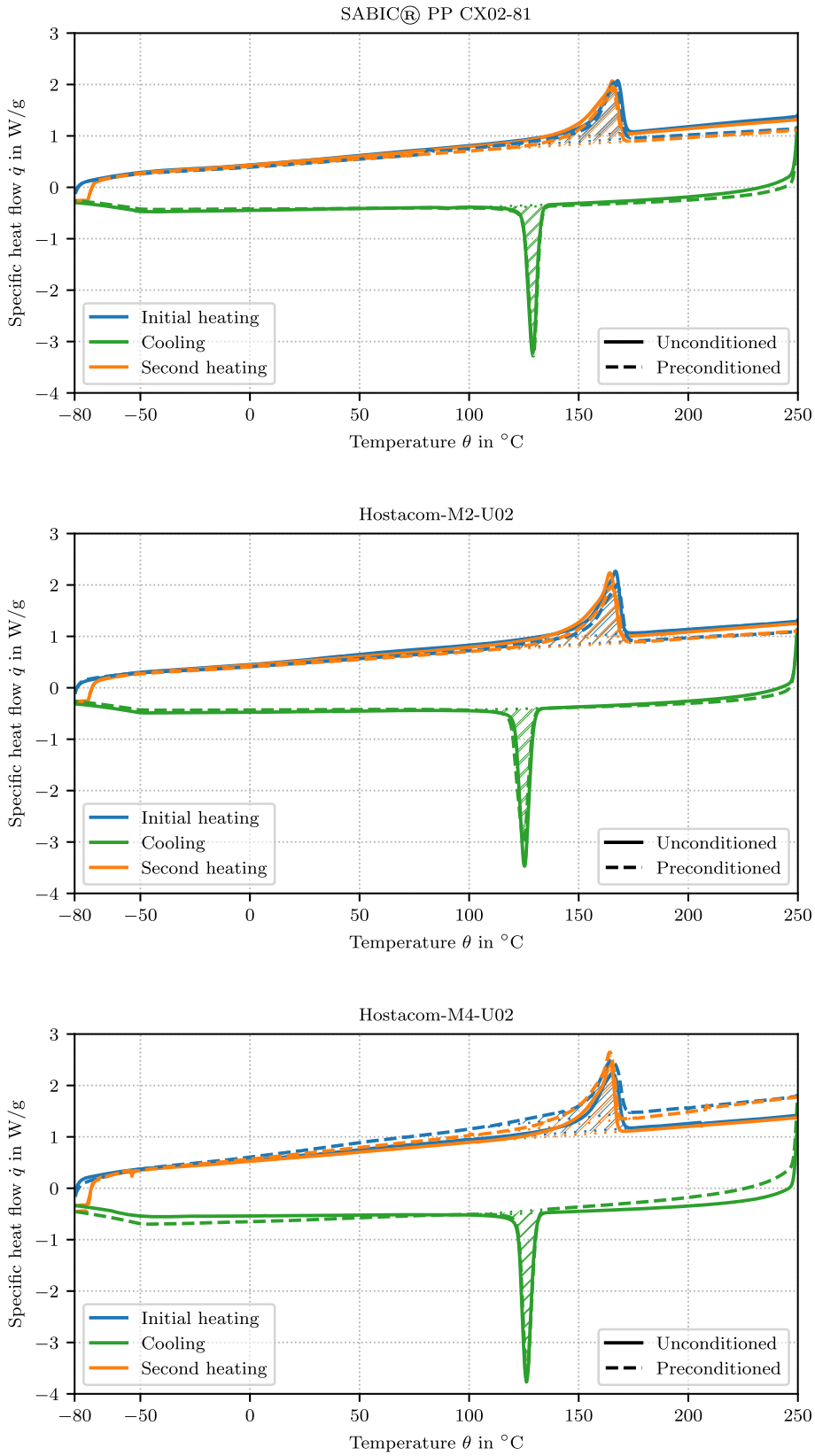

Fig. 8 Mass-specific heat-flow rate $\dot{q}(\theta)$ obtained from DSC measurements for all materials, incorporating both the unconditioned and preconditioned samples. Each experiment consisted of an initial heating run (blue), a subsequent cooling run (green), and a second heating run (orange). The region designated for the evaluation of enthalpy of melting is delineated by the hatched area

Acknowledgements The research presented in this paper was conducted as part of an industrial Ph.D. project at Dr. Ing. h.c. F. Porsche AG, whose support is greatly appreciated. The authors would also like to express their gratitude to their colleagues from both KIT and Porsche for their insightful discussions and technical assistance during the experiments. We would like to express our profound gratitude to Julian Baldauf for his invaluable guidance and training on the experimental equipment, to Martin Schwedes for conducting the DSC measurements at TU Clausthal, and to Johannes Keursten for his meticulous proofreading of the manuscript.

Author Contributions Yiheng Huang: Writing-original draft, Conceptualization, Investigation, Experiments, Formal analysis, Visualization. Loredana Kehrer: Writing-editing and review, Supervision of experiments. Valerian Hirschberg: Writing-editing and review, Supervision of experiments. Eike Reinhardt: Writing-editing and review, Project administration. Frank Burbulla: Writing-editing and review, Project administration. Thomas Böhlke: Writing-editing and review, Supervision.

Data availability Raw data will be made available on request.

Declarations

Conflict of interest The authors declare that they have no conflict of interest.

Ethical approval This article does not contain any studies with human participants or animals performed by any of the authors.

Appendix A Assessment of sample consistency and quality based on dilatometry tests

Figure 9 shows the mean value and standard deviation of three different samples of SABIC®-PP-CX02-81 tested under the same experimental settings, with the only difference being that one sample was tested only up to 80 °C. Nevertheless, it is evident that the samples deviate only minimally from one another. For clarification, two of the samples were taken from the same plate but from different positions, while the third sample originated from an entirely different plate.

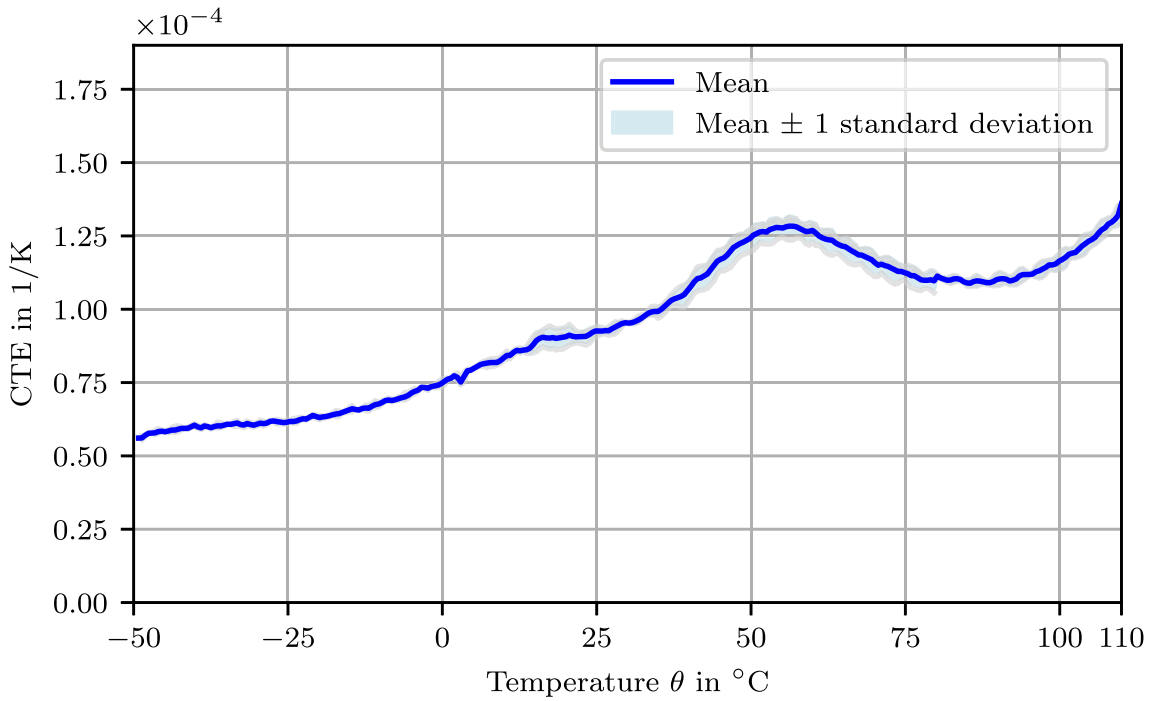

Fig. 9 Mean CTE, cf. Equation 2, for three samples of SABIC®-PP-CX02-81

References

1. Agarwal, J., Sahoo, S., Mohanty, S., Nayak, S.K.: Progress of novel techniques for lightweight automobile applications through innovative eco-friendly composite materials: A review. J. Thermoplast. Compos. Mater. **33**(7), 978–1013 (2020). https://doi.org/10.1177/0892705718815530. (**Accessed 2025-09-13**)
2. Al-Ali AlMa'adeed, M., Krupa, I. (eds.): Polyolefin Compounds and Materials: Fundamentals and Industrial Applications. Springer Series on Polymer and Composite Materials. Springer, Cham (2016). https://doi.org/10.1007/978-3-319-25982-6 . Accessed 2025-09-13
3. Miller, L., Soulliere, K., Sawyer-Beaulieu, S., Tseng, S., Tam, E.: Challenges and alternatives to plastics recycling in the automotive sector. Materials **7**(8), 5883–5902 (2014). https://doi.org/10.3390/ma7085883. (**Accessed 2025-09-13**)
4. Malacari, P.E., Spa, I.: Talc in automotive applications. NAFTA 12, 58 (2009). Accessed 14 September 2025
5. Nurul, M.S., Mariatti, M.: Effect of hybrid nanofillers on the thermal, mechanical, and physical properties of polypropylene composites. Polym. Bull. **70**(3), 871–884 (2013). https://doi.org/10.1007/s00289-012-0893-9. (**Accessed 2025-07-24**)
6. Wasel, M.A., Wassel, A.R., Sewid, F.A., El-Tonsy, M.M., El-Henawey, M.I.: Enhanced thermal stability and mechanical properties of polypropylene matrices reinforced with SiO_2 nanoparticles. Phys. Scr. **100**(3), 035931 (2025). https://doi.org/10.1088/1402-4896/adb245. (**Accessed 2025-08-13**)
7. Lapcik, L., Jindrova, P., Lapcikova, B., Tamblyn, R., Greenwood, R., Rowson, N.: Effect of the talc filler content on the mechanical properties of polypropylene composites. J. Appl. Polym. Sci. **110**(5), 2742–2747 (2008). https://doi.org/10.1002/app.28797. (**Accessed 2025-09-01**)
8. Li, J., Zhu, Z., Li, T., Peng, X., Jiang, S., Turng, L.: Quantification of the Young's modulus for polypropylene: Influence of initial crystallinity and service temperature. J. Appl. Polym. Sci. **137**(16), 48581 (2020). https://doi.org/10.1002/app.48581. (**Accessed 2025-08-14**)
9. Zuidema, H., Peters, G.W.M., Meijer, H.E.H.: Influence of cooling rate on pVT-data of semicrystalline polymers. J. Appl. Polym. Sci. **82**(5), 1170–1186 (2001). https://doi.org/10.1002/app.1951. (**Accessed 2025-08-14**)
10. Hu, Y., Liao, Y., Zheng, Y., Ikeda, K., Okabe, R., Wu, R., Ozaki, R., Xu, J., Xu, Q.: Influence of cooling rate on crystallization behavior of semi-crystalline polypropylene: Experiments and mathematical modeling. Polymers **14**(17), 3646 (2022). https://doi.org/10.3390/polym14173646. (**Accessed 2025-08-14**)
11. Gaspar-Cunha, A., Melo, J., Marques, T., Pontes, A.: A review on injection molding: Conformal cooling channels, modeling, surrogate models, and multi-objective optimization. Polymers **17**(7), 919 (2025). https://doi.org/10.3390/polym17070919. (**Accessed 2025-09-01**)
12. Kościuszko, A., Marciniak, D., Sykutera, D.: Post-processing time dependence of shrinkage and mechanical properties of injection-molded polypropylene. Materials **14**(1), 22 (2020). https://doi.org/10.3390/ma14010022. (**Accessed 2025-08-14**)
13. Gahleitner, M., Fiebig, J., Wolfschwenger, J., Dreiling, G., Paulik, C.: Post-crystallization and physical aging of polypropylene: Material and processing effects. J. Macromol. Sci. Part B **41**(4–6), 833–849 (2002). https://doi.org/10.1081/MB-120013068. (**Accessed 2025-08-08**)
14. Velasco, J.I., De Saja, J.A., Martínez, A.B.: Crystallization behavior of polypropylene filled with surface-modified talc. J. Appl. Polym. Sci. **61**(1), 125–132 (1996)
15. Castillo, L.A., Barbosa, S.E.: Comparative analysis of crystallization behavior induced by different mineral fillers in polypropylene nanocomposites. Nanomater. Nanotech. **10**, 184798042092275 (2020)
16. Branciforti, M.C., Oliveira, C.A., De Sousa, J.A.: Molecular orientation, crystallinity, and flexural modulus correlations in injection molded polypropylene/talc composites. Polym. Adv. Technol. **21**(5), 322–330 (2010). https://doi.org/10.1002/pat.1431. (**Accessed 2026-02-21**)
17. Bajsić, E.G., Rek, V., Pavić, B.O.: The influence of talc content on the thermal and mechanical properties of thermoplastic polyurethane/polypropylene blends. J. Elastom. & Plastics **45**(6), 501–522 (2013). https://doi.org/10.1177/0095244312458602. (**Accessed 2025-07-24**)
18. Zhou, Y., Rangari, V., Mahfuz, H., Jeelani, S., Mallick, P.K.: Experimental study on thermal and mechanical behavior of polypropylene, talc/polypropylene and polypropylene/clay nanocomposites. Mater. Sci. Eng., A **402**(1–2), 109–117 (2005). https://doi.org/10.1016/j.msea.2005.04.014. (**Accessed 2025-07-24**)
19. Ellis, T.S., D'Angelo, J.S.: Thermal and mechanical properties of a polypropylene nanocomposite. J. Appl. Polym. Sci. **90**(6), 1639–1647 (2003). https://doi.org/10.1002/app.12830. (**Accessed 2025-07-24**)
20. Jourdan, C., Cavaille, J.Y., Perez, J.: Mechanical relaxations in polypropylene: a new experimental and theoretical approach. J. Polym. Sci., Part B: Polym. Phys. **27**(11), 2361–2384 (1989). https://doi.org/10.1002/polb.1989.090271115. (**Accessed 2025-08-01**)
21. Read, B.E.: Mechanical relaxation in isotactic polypropylene. Polymer **30**(8), 1439–1445 (1989). https://doi.org/10.1016/0032-3861(89)90213-9. (**Accessed 2025-07-24**)
22. Pae, K.D., Sauer, J.A.: Effects of thermal history on isotactic polypropylene. J. Appl. Polym. Sci. **12**(8), 1901–1919 (1968). https://doi.org/10.1002/app.1968.070120811. (**Accessed 2026-02-21**)
23. Lima, M.F.S., Vasconcellos, M.A.Z., Samios, D.: Crystallinity changes in plastically deformed isotactic polypropylene evaluated by x-ray diffraction and differential scanning calorimetry methods. J. Polym. Sci., Part B: Polym. Phys. **40**(9), 896–903 (2002). https://doi.org/10.1002/polb.10159. (**Accessed 2026-02-21**)
24. Material Data Center Datenblatt für SABIC® PP CX02-81 - PP - Saudi Basic Industries Corporation (SABIC). https://www.materialdatacenter.com/ms/de/tradenames/Sabic/Saudi+Basic+Industries+Corporation+%28SABIC%29/SABIC+PP+CX02-81/2028d1a7/2171 Accessed 27 January 2026
25. Material Data Center Datenblatt für Hostacom M2 U02 102942 - PP-T20 - LyondellBasell Industries. https://www.materialdatacenter.com/ms/de/tradenames/Hostacom/LyondellBasell+Industries/Hostacom+M2+U02+102942/c401478c/314 Accessed 27 January 2026
26. Material Data Center Datenblatt für Hostacom M4 U02 102943 - PP-T40 - LyondellBasell Industries. https://www.materialdatacenter.com/ms/de/tradenames/Hostacom/LyondellBasell+Industries/Hostacom+M4+U02+102943/74396cae/314 Accessed 27 January 2026

27. Menard, K.P., Menard, N.R.: Dynamic Mechanical Analysis, 3rd edn. CRC Press, Boca Raton, Fla. (2020). https://doi.org/10.1201/9780429190308. https://www.taylorfrancis.com/books/9781482255522 Accessed 07 August 2025
28. Brinson, H.F., Brinson, L.C.: Polymer Engineering Science and Viscoelasticity: An Introduction. Springer, Boston, MA (2015). https://doi.org/10.1007/978-1-4899-7485-3. https://link.springer.com/10.1007/978-1-4899-7485-3 Accessed 07 August 2025
29. Wunderlich, B.: Thermal Analysis of Polymeric Materials. Springer, Berlin/Heidelberg (2005). https://doi.org/10.1007/b137476 . http://link.springer.com/10.1007/b137476 Accessed 2026-02-03
30. Höhne, G.W.H., Hemminger, W.F., Flammersheim, H.-J.: Differential Scanning Calorimetry. Springer, Berlin, Heidelberg (2003). https://doi.org/10.1007/978-3-662-06710-9 . http://link.springer.com/10.1007/978-3-662-06710-9 Accessed 2026-02-25
31. Ehrenstein, G.W., Riedel, G., Trawiel, P.: Thermal Analysis of Plastics: Theory and Practice. Hanser publ, Munich (2004)
32. Lanyi, F.J., Wenzke, N., Kaschta, J., Schubert, D.W.: On the Determination of the Enthalpy of Fusion of α -Crystalline Isotactic Polypropylene Using Differential Scanning Calorimetry, X-Ray Diffraction, and Fourier-Transform Infrared Spectroscopy: An Old Story Revisited. Adv. Eng. Mater. **22**(9), 1900796 (2020). https://doi.org/10.1002/adem.201900796. (**Accessed 2026-02-03**)
33. DIN EN ISO 11357-1:2023-06, Kunststoffe_- Dynamische Differenzkalorimetrie_(DSC)_- Teil_1: Allgemeine Grundlagen (ISO_11357-1:2023); Deutsche Fassung EN_ISO_11357-1:2023. DIN Media GmbH (2023). https://doi.org/10.31030/3427674. https://www.dinmedia.de/de/-/-/366263770. Accessed 2026-02-09
34. Ono, M., Washiyama, J., Nakajima, K., Nishi, T.: Anisotropy in Thermal Expansion in Rubber Toughened Polypropylene —Injection Molded System—. Polym. J. **36**(7), 563–566 (2004). https://doi.org/10.1295/polymj.36.563. (**Accessed 2026-07-28**)
35. Cho, K., Saheb, D.N., Choi, J., Yang, H.: Real time in situ X-ray diffraction studies on the melting memory effect in the crystallization of β-isotactic polypropylene. Polymer **43**(4), 1407–1416 (2002). https://doi.org/10.1016/S0032-3861(01)00729-7. (**Accessed 2025-09-12**)
36. Ehrenstein, G.W.: Polymer-Werkstoffe: Struktur - Eigenschaften - Anwendung, 3. auflage edn. Hanser eLibrary. Hanser, München (2011). https://doi.org/10.3139/9783446429673
37. Ferry, J.D.: Viscoelastic Properties of Polymers, 3d, edn. Wiley, New York (1980)
38. Tajvidi, M., Falk, R.H., Hermanson, J.C.: Effect of natural fibers on thermal and mechanical properties of natural fiber polypropylene composites studied by dynamic mechanical analysis. J. Appl. Polym. Sci. **101**(6), 4341–4349 (2006). https://doi.org/10.1002/app.24289. (**Accessed 2025-07-24**)
39. Gahleitner, M., Grein, C., Bernreitner, K., Knogler, B., Hebesberger, E.: The use of DMTA for predicting standard mechanical properties of developmental polyolefins. J. Therm. Anal. Calorim. **98**(3), 623–628 (2009). https://doi.org/10.1007/s10973-009-0506-5. (**Accessed 2025-09-06**)
40. Fiebig, J., Gahleitner, M., Paulik, C., Wolfschwenger, J.: Ageing of polypropylene: processes and consequences. Polym. Testing **18**(4), 257–266 (1999). https://doi.org/10.1016/S0142-9418(98)00023-3. (**Accessed 2025-09-06**)